JOURNAL OF THE ROYAL SOCIETY Interface

Hummingbird wing efficacy depends on aspect ratio and compares with helicopter rotors

Jan W. Kruyt, Elsa M. Quicazán-Rubio, GertJan F. van Heijst, Douglas L. Altshuler and David Lentink

J. R. Soc. Interface 2014 **11**, 20140585, published 30 July 2014

JOURNAL OF THE ROYAL SOCIETY Interface

rsif.royalsocietypublishing.org

Research

Cite this article: Kruyt JW, Quicazán-Rubio EM, van Heijst GJF, Altshuler DL, Lentink D. 2014 Hummingbird wing efficacy depends on aspect ratio and compares with helicopter rotors. *J. R. Soc. Interface* **11**: 20140585. http://dx.doi.org/10.1098/rsif.2014.0585

Received: 2 June 2014
Accepted: 7 July 2014

Subject Areas:
biomechanics, biomimetics

Keywords:
hovering, hummingbird, quasi-steady, performance, wing, aspect ratio

Author for correspondence:
David Lentink
e-mail: dlentink@stanford.edu

Electronic supplementary material is available at http://dx.doi.org/10.1098/rsif.2014.0585 or via http://rsif.royalsocietypublishing.org.

Royal Society Publishing

Hummingbird wing efficacy depends on aspect ratio and compares with helicopter rotors

Jan W. Kruyt[1,2], Elsa M. Quicazán-Rubio[2], GertJan F. van Heijst[3], Douglas L. Altshuler[4] and David Lentink[1]

[1]Mechanical Engineering, Stanford University, 416 Escondido Mall, Stanford, CA 94305, USA
[2]Experimental Zoology Group, Wageningen University, PO Box 338, 6700 AH Wageningen, The Netherlands
[3]Physics Department, Eindhoven University of Technology, PO Box 516, 5600 MB Eindhoven, The Netherlands
[4]Department of Zoology, University of British Columbia, 4200-6270 University Boulevard, Vancouver, British Columbia, Canada V6T1Z4

Hummingbirds are the only birds that can sustain hovering. This unique flight behaviour comes, however, at high energetic cost. Based on helicopter and aeroplane design theory, we expect that hummingbird wing aspect ratio (AR), which ranges from about 3.0 to 4.5, determines aerodynamic efficacy. Previous quasi-steady experiments with a wing spinner set-up provide no support for this prediction. To test this more carefully, we compare the quasi-steady hover performance of 26 wings, from 12 hummingbird taxa. We spun the wings at angular velocities and angles of attack that are representative for every species and measured lift and torque more precisely. The power (aerodynamic torque × angular velocity) required to lift weight depends on aerodynamic efficacy, which is measured by the power factor. Our comparative analysis shows that AR has a modest influence on lift and drag forces, as reported earlier, but interspecific differences in power factor are large. During the downstroke, the power required to hover decreases for larger AR wings at the angles of attack at which hummingbirds flap their wings ($p < 0.05$). Quantitative flow visualization demonstrates that variation in hover power among hummingbird wings is driven by similar stable leading edge vortices that delay stall during the down- and upstroke. A side-by-side aerodynamic performance comparison of hummingbird wings and an advanced micro helicopter rotor shows that they are remarkably similar.

1. Introduction

Hovering hummingbirds exhibit the highest contractile frequencies of any vertebrate limb muscle [1], surpassed only by some sonic muscles and insect flight muscles [2–4]. This activity requires among the highest mass-specific metabolic input [5] and mechanical power output [6] of any form of locomotion [7]. Hummingbirds exhibit numerous specializations for high metabolism and high wingbeat frequencies such as modifications to the muscular and skeletal systems [8–11]; we expect the wing shape to be no exception. However, the energy-specific effect of variation in wing shape on hummingbird hovering, or indeed for any animal employing flapping flight, has not been established fully.

Wing shape can be described by a number of factors, but the aspect ratio (AR), a dimensionless number defined as the ratio of wing length to wing width, drives the design of engineered flyers in particular [12–15]. This ratio is identical among wings with different width distributions (along their span) when the wing span divided by average wing chord is the same—and higher AR wings are more energy efficient [12–14]. Hummingbird wings are highly variable in size, with wing length ranging from 35 to 152 mm among species [16]. By contrast, AR ranges only from 3 to 4.5 [16,17]. Notably, all hummingbird wings are of much lower AR than the rotor blades and wings selected in aviation design [12,13,15,18].

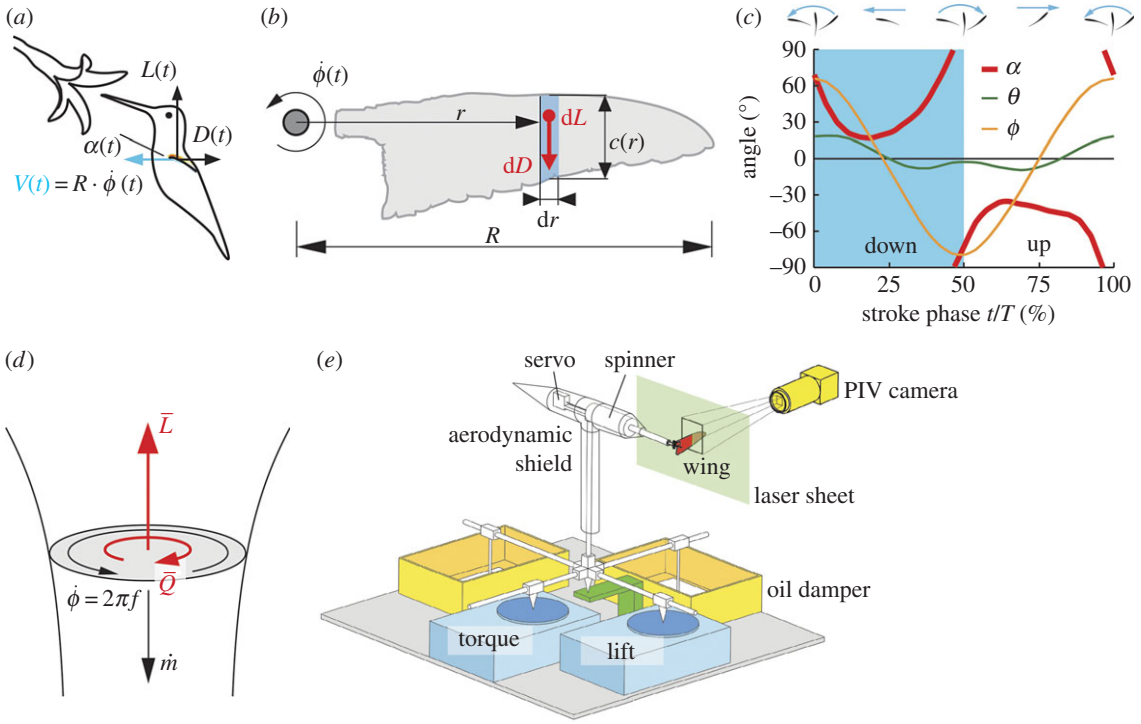

Figure 1. Quasi-steady paradigm for hummingbird hover performance. (*a*) Hovering hummingbird in front of flower, its wings flap with instantaneous velocity $V(t)$ at angle of attack $\alpha(t)$, resulting in aerodynamic lift $L(t)$ and drag $D(t)$. (*b*) Local lift and drag at a wing station of a hummingbird during midstroke (right wing), with wing radius R, local radius r, angular velocity $\dot{\phi}(t)$, chord length $c(r)$. (*c*) Flapping kinematics of an Anna's hummingbird *Calypte anna* in hovering flight with wing stroke angle ϕ, deviation angle θ, and angle of attack α (blue area: downstroke). (*d*) The propeller force coefficients in the quasi-steady model of flapping flight are obtained by spinning the wing (analogous to an actuator disc with mass flow $\dot{m}$ generating mean lift $\bar{L}$ at the cost of mean torque $\bar{Q}$), enabling instantaneous lift and torque estimates as a function of angle of attack. (*e*) Our custom designed spinning wing set-up for force and flow (PIV) measurement. The spinner set-up is aerodynamically shielded, mechanically insulated and oil damped. (Online version in colour.)

Hummingbird hovering kinematics are characterized by high stroke amplitudes [19,20], over which the wing translates for several chord lengths. This feature makes hummingbird hovering kinematics a suitable subject for quasi-steady analysis with revolving wings, in particular during midstroke when wing acceleration is zero and the time-history effects of stroke reversal are weak [21–25]. Previous work on revolving dried hummingbird wings by Altshuler *et al*. [26] demonstrated quasi-steady wing lift coefficients similar to those found on other bird and insect wings [22,24]. Usherwood & Ellington [24] show that at biologically relevant angles of attack, lift coefficients on a range of dried insect, bird and flat model wings are independent of the wing's AR. Owing to imprecise drag measurement, these studies did not quantify the effect of wing shape on drag force (aerodynamic torque per arm) or aerodynamic power (torque × angular velocity). Hence, the influence of wing AR on (quasi-steady) energetics has not been quantified for hovering animals.

Here, we study the effect of AR on aerodynamic lift, drag and power of dried hummingbird wings of 12 species. In this essay, we have also included rotor blades of one of the world's most advanced micro helicopters at hummingbird scale, the ProxDynamics Black Hornet (ProxDynamics, Norway), to compare helicopter and hummingbird. First, we measured the time-averaged lift and drag forces of these wings, while spinning them at constant angular velocity, using a custom-built lift and torque measurement set-up. Second, we studied the flow structure around the wing using phase-locked particle image velocimetry (PIV) at different spanwise stations. We found that hovering forces are similar among the 12 species of hummingbirds (measured for 26 wings) and a micro helicopter rotor. To compare these forces with earlier results for spinning and flapping fly wings, we fit the quasi-steady aerodynamic model for fly wings with our hummingbird data. The quasi-steady model predicts the instantaneous lift and drag based upon the lift and drag force generated by the same wing spinning continuously at the same angular velocity and angle of attack. The quasi-steady harmonic model for fly wings relates lift and drag to angle of attack through sine and cosine functions [21], which fit remarkably well to our lift and drag data too. For positive angles of attack we find, however, that the resultant force is not 90° rotated with respect to the angle of attack. Unlike quasi-steady models for insect wings, the resultant force of hummingbird and micro helicopter wings point more forward, which corresponds to a lower drag during the downstroke. Our measurements and quasi-steady power calculations show that hummingbird wings that spin like helicopter rotors at the optimal angle of attack require less aerodynamic power to hover than calculated for flapping wings using quasi-steady assumptions. Finally, we find that higher AR hummingbird wings require less power to lift body weight.

2. Methods

2.1. Force measurements

To develop a quasi-steady model of hovering hummingbird flight, we developed a wing spinner [21,23–27] to measure wing lift and torque accurately across biologically relevant angles of attack and Reynolds numbers (Reynolds number represents inertial versus viscous effects in the flow). The spinner (figure 1*e*) consists

of an aluminium housing holding two different micromotors (AXi2212/34 and AXi2208/20 model motors) mounted onto a single hollow axle, giving a combined dynamic range of 500–11 000 r.p.m. without load. The micromotors were controlled using an electronic speed controller (M-Drive-18, Motortron System Inc.) and a servo board (ServoCenter 3.1, Yost Engineering). A custom-built variable pitch propeller mechanism at the end of the spinning axle rotated the wing around its length axis, controlling the geometrical angle of attack of the wing with respect to the stroke plane. An RC servo (DS281 11 mm, Graupner SJ/GmbH) at the back of the spinner actuated this angle of attack via a push–pull rod through the hollow spinning axle. Different wings were fitted onto the spinner via square-tube mounts attached to the wing root (described in detail below). The variable pitch propeller mechanism was designed such that the wing root was as close as possible to the spinning axle, resulting in a 9.5 mm offset between the axle's centre of rotation and the wing root. This offset approximates the 4.0 mm (s.d. 0.6 mm) offset we measured for five *Calypte anna* wings.

The spinner was mounted onto a stiff and lightweight carbon fibre balancing frame resting on three sharp points: a pivoting point supporting most of the frame's weight, and two points resting onto weighing scales (Adventurer Pro, Ohaus: 210 g range, $\pm$ 0.001 g, 5–6 Hz USB sampling), via saw blade springs mounted on the scale. Movable weights were used to tune the balance frame's centre of gravity such that it coincided with the pivot point, and a preloading mass was applied to keep the sharp points in contact with the weighing scale at all times during the measurement. Thin wires were connected close to the balance's central pivoting point for power supply (7.4VDC, DPS-2010PFC, Voltcraft) and for RS232 communication with a computer.

The measurement accuracy and repeatability of the spinner set-up were improved through several design iterations. To mechanically isolate the set-up from the building, the set-up was placed on a heavy granite table supported by rubber dampers. Vibrations from the spinner itself were damped using a rubber-plated motor suspension and averaged out using custom-built silicon oil dampers (10 000 cSt polydimethylsiloxane, Tribolub). Plastic cowlings resting on separate supports were used to shield the set-up from the propeller wake. Custom Matlab software (v2009a, Mathworks) controlled the wing spinner and read the weighing scales autonomously, taking measurements over a predefined range of spinning frequencies and angles of attack. A frequency search algorithm controlled motor power to maintain the desired spinning frequency under different loading conditions by continuously reading frequency from the electronic speed controller. Autonomous operation of the set-up eliminated handling of the sensitive set-up during measurements taken on each wing.

To calibrate the set-up, we connected horizontal wires to the spinner and ran these over nearly frictionless pulleys to apply a known force and a pure torque using weights. Calibration lift force was applied along the spinning axis at the centre of the spinning axle. For applying calibration torque without net force, we mounted a vertical arm onto the spinner housing, close to the wing's location, sticking both upward and downward from the housing. Wires in opposite directions were then connected to the upper and lower ends of this arm to apply identical but opposing known forces using weights, resulting in a pure torque. In this way, we constructed a 5×5 calibration matrix to translate the measured reaction forces into lift and torque exerted by the wing, while compensating for effects of coupled loading. The calibrations were repeated five times before and after testing all hummingbird wings. Two separate corrections were applied in addition, one to account for the balance's centre of gravity shift under different servo positions used for controlling the wing's angle of attack, and a second to account for the effect of mechanical and aerodynamic friction on the rotating parts of the set-up, including the plastic wing mounts. These corrections were performed immediately after each measurement and subtracted from the signal. The resulting overall accuracy is 6.5% for torque (drag) and 1.4% for thrust (lift) for all measurements. Force measurements are less precise for small angles of attack between -4° and 4°. Force gradient is less precise at 0° where measurements for negative and positive angles of attack connect.

In total, we selected wings from 12 hummingbird species, representing five of the nine hummingbird clades [28], to maximize morphological variety. Colombian hummingbird wings ($n = 54$) were loaned from the museum collection of the Instituto de Ciencias Naturales of the Universidad Nacional de Colombia and sent to Wageningen University. In addition, seven male Anna's hummingbirds (*C. anna*), euthanized for other studies at the University of California, Riverside, were stored frozen in good condition. After careful preparation, their wings were donated to the Museum of Vertebrate Zoology at the University of California, Berkeley, and subsequently loaned from the University of California, Berkeley to Wageningen University. The *C. anna* wings ($n = 11$) we loaned for our study originated from birds for which all animal procedures were approved by the Institutional Animal Care and Use Committee of the University of California, Riverside. All wings were dried in fully stretched (spread) configuration to closely resemble the wing shape during downstroke observed in high-speed videos of hovering hummingbirds. Each wing was provided with a square plastic mount lined up with the last secondary feather, and carefully groomed using an entomological pin. Because we tested single hummingbird wing performance with the spinner, each wing's out-of-centre mass on the spinning axle was balanced with a counterweight of small lead fishing weights on a plastic mount. We made a selection from the collection of wings by first favouring wings that were not moulting and were not damaged during preparation, and then for male specimens and right wings, and finally for minimal imperfections. We selected five wings for Anna's hummingbird (*C. anna*), and between one and three wings for all other species (figure 2). Although wing spread varies somewhat between wings owing to the drying process, wing preparation has been significantly improved compared with earlier hummingbird studies [26]. The most parsimonious interpretation of the performance differences reported in this study is therefore in relation to geometrical differences in wing morphology, in particular wing AR. We also took force measurements on a single high-performance carbon fibre model helicopter for comparison. This rotor design was used to power the ProxDynamics Black Hornet micro helicopter, a reconnaissance micro helicopter of hummingbird size. The micro helicopter has a carbon fibre rotor with 52 mm radius, about 6.5% camber and 5.5° wing twist.

Lift and torque were measured for a wide range of biologically relevant angles of attack at three constant angular velocities per wing. The angles of attack ranged from -90° to 90° (120 measurement angle steps) for three wings of *C. anna* and from -45° to 45° (78 angle steps) for the 23 remaining wings of 12 different species, as well as for the model helicopter wing. The geometrical angle of attack α_{geo} step size was selected to be 1° for $-25^\circ \leq \alpha_{geo} \leq 25^\circ$ to better resolve low drag values compared with earlier studies [23–27]. For $-25^\circ > \alpha_{geo} > 25^\circ$, a 3° step size was sufficient. For every wing, we first increased and then decreased the angle of attack and repeated this three times; we found minimal hysteresis, so we effectively repeated every experiment six times. At every angle of attack, we recorded the forces 100 times at a 5–6 Hz sample rate, resulting in 600 samples for every angle of attack in total. We define the 0° aerodynamic angle of attack as the angle that gives zero lift. Because the set-up has been calibrated for static measurements, resulting in a static transfer function that relates displacement to force, we checked whether the balance attained static conditions. We used the fast Fourier transform (FFT) to compute the dynamic power present in the frequency

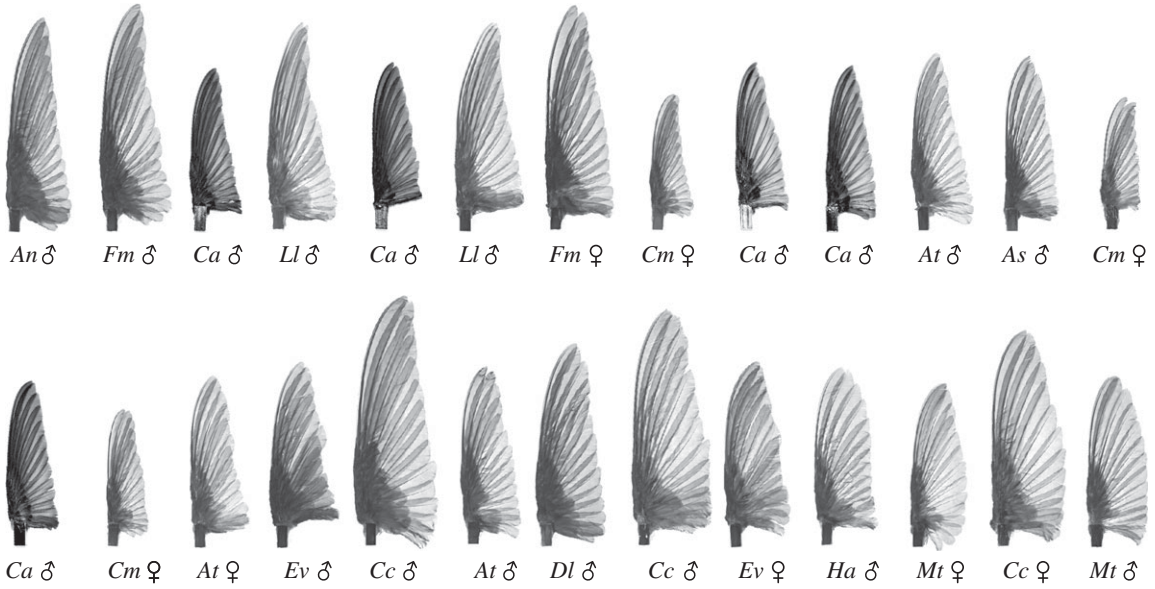

Figure 2. Dried hummingbird wings ranked from highest to lowest AR (left to right, top to bottom). Each wing was mounted on a plastic square tube. *An*, *Anthracothorax nigricollis*, *At*, *Amazilia tzacatl*, *As*, *Amazilia saucerottei*, *Ca*, *Calypte anna*, *Cc*, *Colibri coruscans*, *Cm*, *Chaetocercus mulsant*, *Dl*, *Doryfera ludovicae*, *Ev*, *Eriocnemis vestita*, *Fm*, *Florisuga mellivora*, *Ha*, *Haplophaedia aureliae*, *Ll*, *Lafresnaya lafresnayi*, *Mt*, *Metallura tyrianthina*.

spectrum below 1 Hz (at higher frequencies, the power was negligible) in both the lift and torque measurements (electronic supplementary material, figures S1 and S2). Based on this evaluation, we found that the torque measurements did not reach static equilibrium for angles beyond 35° making these values less precise. Comparison of our torque values with values published for hummingbird and other bird wings suggests that our results are of similar or better quality [26,27,29].

The hummingbird stroke angle is approximately sinusoidal, corresponding to sinusoidal angular velocity ($\dot{\phi}(t)$), figure 1*c*. Three tip velocities were selected for each wing to represent three characteristic wingtip Reynolds numbers, and loading cases, during the wing stroke (figure 5*a*). The wing loading, measured in G (lift/weight), varies with normalized velocity squared throughout the stroke. We tested the wings for three characteristic loading cases: 1G, which represents the average wing loading during hovering (lift = weight), 2G, which represents the maximum wing loading during midstroke and 0.5G which represents a lower loading case closer to stroke reversal. The corresponding angular velocities were calculated based on the measured flapping frequency and amplitude of nine hummingbird species [16,30,31] assuming a sinusoidal wing stroke (figure 1*c* and see parameters in the electronic supplementary material, tables S1 and S2). For three species (*Anthracothorax nigricollis*, *Eriocnemis vestita* and *Haplophaedia aureliae*), such measurements were not reported in literature, instead, we estimated angular velocities of these species assuming an average 1G lift coefficient of $\overline{C_L} = 1.5$ (see the electronic supplementary material). The Reynolds numbers corresponding to each loading condition were computed for each wing based on air density ρ and viscosity μ, as well as wing tip velocity V_{tip} and the wing's mean chord length $\bar{c}$

$$Re = \frac{\rho V_{tip} \bar{c}}{\mu}. \tag{2.1}$$

Using Reynolds number, wing length R, and the wing root offset from the spinning axis d, we computed the three (constant) spinning frequencies f corresponding with every G-loading as follows

$$f_G = \frac{\dot{\phi}_G}{2\pi} = \frac{V_{tip,G}}{2\pi(R+d)} = \frac{\mu Re_G}{2\pi\rho\bar{c}(R+d)}. \tag{2.2}$$

2.2. Calculation of force coefficients and power factor

During hovering flight, there is no forward velocity, and therefore the appropriate direction of the lift vector is perpendicular to the velocity direction of the wing stroke itself and aerodynamic torque owing to drag is parallel to stroke velocity (figure 1*a*,*d*). Following Weis-Fogh and others [23,32,33], we use the blade element model for animal flight to calculate time-averaged lift and drag coefficients. The model sums up all lift and torque contributions acting on infinitesimally thin blade elements along the wing length R, throughout a stroke of period T

$$\bar{L} = \frac{1}{T}\int_0^T \int_0^R C_l(r,t)\frac{1}{2}\rho[\dot{\phi}(t)r]^2 c(r)\,\mathrm{d}r\,\mathrm{d}t \tag{2.3}$$

and

$$\bar{Q} = \frac{1}{T}\int_0^T \int_0^R C_d(r,t)\frac{1}{2}\rho[\dot{\phi}(t)r]^2 c(r) r\,\mathrm{d}r\,\mathrm{d}t. \tag{2.4}$$

The local blade element area is the product of local wing chord $c(r)$ and infinitesimal wingspan dr. The dynamic pressure acting on this area is a function of local radius r. The corresponding lift and drag coefficients for the wing spinner at angular velocity $\dot{\phi} = 2\pi f$ are

$$C_L = \frac{2\bar{L}}{\rho[2\pi f]^2 R_2{}^2 S} \tag{2.5}$$

and

$$C_D = \frac{2\bar{Q}}{\rho[2\pi f]^2 R_3{}^3 S}. \tag{2.6}$$

Here R_2 and R_3 are the second and third moments of area, respectively, that account for the velocity gradient along wingspan

$$R_2 = \sqrt{\frac{1}{S}\int_0^R r^2 c(r)\,\mathrm{d}r} \tag{2.7}$$

and

$$R_3 = \sqrt[3]{\frac{1}{S}\int_0^R r^3 c(r)\,\mathrm{d}r} \tag{2.8}$$

The force coefficients calculated from the spinner data (C_L, C_D) can be fed back into the original blade element model to make

quasi-steady estimates for the time-averaged lift and torque (electronic supplementary material, equations S.16 and S.18) of a hummingbird in hovering flight [21,34].

Previous quasi-steady models do not account for Reynolds number variation within a stroke [21,24,25,27,34], which is reasonable, because these effects are small for flapping rigid wings [35]. The effect on deformable wings [36,37] might, however, be pronounced, because wing loading is proportional to velocity squared (which scales with Reynolds number squared). Throughout the wing stroke, the wing undergoes different G-loading (lift/weight) conditions. The average wing loading is 1G for hover (figure 5*a*). To compare force coefficients among individuals while accounting for both Reynolds number and wing deformation effects, we average the force coefficients over wings under 0.5, 1 and 2G loading. The individual coefficients are dynamically weighted with velocity squared within a sinusoidal stroke: $Re_{0.5G} = 11\%$; $Re_{1G} = 28\%$; $Re_{2G} = 61\%$. The weighted average is closest to the midstroke condition for which G-loading is 2, and Reynolds number maximal. The corresponding standard deviation was computed by similar dynamic weighting of the standard deviation contributions of each G-loading case.

Whereas lift and drag coefficients give insights into aerodynamic performance, they do not individually quantify energetic performance—the aerodynamic power required to lift body weight:

$$\overline{P_{\text{aero}}} = \overline{DV} = \overline{Q\dot{\phi}} = \frac{1}{T}\int_0^T \int_0^R C_{\text{d}}(r,t)\frac{1}{2}\rho\dot{\phi}^3 r^3 c(r)\,\text{d}r\,\text{d}t, \tag{2.9}$$

which simplifies into (using equation (2.8)):

$$\overline{P_{\text{aero}}} = \frac{1}{2}\rho[2\pi f]^3 C_{\text{D}} {R_3}^3 S. \tag{2.10}$$

During hovering flight, the flapping frequency must be sufficiently high such that the lift supports the body weight ($\bar{L} = W$). Flapping frequency must therefore be equal to

$$f = \sqrt{\frac{W}{\frac{1}{2}\rho[2\pi]^2 C_{\text{L}} {R_2}^2 S}}. \tag{2.11}$$

Combining equation (2.10) and (2.11) enables us to calculate aerodynamic power and identify how it depends on drag and lift coefficient

$$\overline{P_{\text{aero}}} = W^{\frac{3}{2}} \frac{{R_3}^3}{{R_2}^3}\sqrt{\frac{2}{\rho S}}\sqrt{\frac{\overline{{C_{\text{D}}}^2}}{\overline{{C_{\text{L}}}^3}}}. \tag{2.12}$$

The aerodynamic power is thus proportional to the power factor [38]

$$\text{PF} = \sqrt{\frac{\overline{{C_{\text{L}}}^3}}{\overline{{C_{\text{D}}}^2}}}. \tag{2.13}$$

The power factor, PF, is a measure of the aerodynamic efficacy (the effectiveness) of the wing, because it measures how much weight can be lifted per unit of aerodynamic power. Because power is proportional to the inverse of PF, the required aerodynamic power is lower for higher power factors. The power factor, therefore, enables us to quantify energy efficacy of hummingbird wings as a function of their AR. Because the power factor represents a gradient of the force coefficients, it is sensitive to noise amplification, and thus requires smoothing of the variables used to calculate it. To obtain precise values, we applied a penalized least-squares smoothing algorithm [39] and applied it to the lift and drag coefficients versus angle of attack. Based on these values, we computed the power factor for each angle of attack.

2.3. Particle imaging velocimetry

To understand the aerodynamic basis for energy efficacy, we performed quantitative flow measurement around the wings using phase-locked, planar PIV. To track airflow, we seeded the room with microscopic fog particles using a smoke generator (VDP900HZ, HQ power). The particles were illuminated using a light sheet on the upper and lower side generated by a laser (Dual SL454–10-OPG, Spectron Laser Systems, flashlamp pumped Nd:YAG laser, 532 nm, 200 mJ pulse^{-1}, 13 ns pulse duration, 15 Hz repetition rate). The laser created a single beam that was split up using mirror optics to illuminate the wing's lower and upper surface, practically eliminating shadow effects. We focused a PIV camera (MegaPlusII ES 2020, Redlake, 30 fps, 1600 × 1200 pixels) with a 105 mm zoom lens (Nikkor Micro, Nikon) on the laser sheet to record particle motion around selected hummingbird wings and the micro helicopter blade. The wings were fixed to the spinner and spun one by one. A tachometer (PLT200, Monarch Instrument) was used to trigger the laser pulse and the camera exposure as the wing passed through the laser sheet and the camera looked along the wing span. We tested wings from eight different species (*A. saucerottei*, *A. tzacatl*, *C. anna*, *C. coruscans*, *C. mulsant*, *D. ludovicae*, *L. lafresnayi*, *M. tyrianthina*). We selected the individuals of every species that produced a lift–drag polar closest to its species-average. We made recordings at 20–22 equidistant spanwise recording stations (step sizes for each individual ranging from 2 to 3.1 mm) from wing root to well beyond the tip. The spanwise positions were sampled by traversing the spinner set-up with respect to the laser sheet using a computer-controlled linear actuator (custom design by Motion Control Technics using 5 mm per stroke ball screw, AMS AM34–420–2-EFB stepper motor and AMS MAX-410 controller). For each station, we recorded 25 phase-locked image pairs.

To obtain flow fields, the particle image pairs were cross-correlated using DaVis particle image velocimetry software (DaVis v. 7.4, LaVision GmbH). Based on visual inspection of the raw data, we first selected the wing stations of interest: 25%, 50% and 75% span. We then used a multi-pass cross-correlation procedure with grid refinement, consisting of a first pass on a 128 × 128 pixel grid (0% overlap) and then two passes on a finer 64 × 64 pixel grid (75% overlap) [40]. A universal outlier detection was used to filter out spurious vectors, which were replaced by interpolated vectors. Algorithmic masks were used to restrict cross-correlation to the parts of the velocity field where particle visibility was not impaired by background reflections. Finally, we time-averaged velocity fields over 25 phase-locked snapshots.

2.4. Wingbeat kinematics of *Calypte anna*

Anna's hummingbirds were recorded during hovering in front of an artificial feeder in a flight chamber. The chamber was composed of three clear acrylic sheets and three white opaque acrylic sheets. Three high-speed cameras (Photron APX) recorded at 1000 frames per second. The cameras were placed orthogonally and filmed through the clear acrylic with the white acrylic as background. Body positions and wingbeat kinematics were digitized frame by frame and averaged using custom software programmed in Matlab by Fry *et al*. [41]. We selected kinematics of three individuals; one moulting male juvenile and two females.

3. Results and discussion

Hovering hummingbirds generate stable leading edge vortices [42,43] that enable their wings to operate at high angles of attack using delayed stall [44]. Our measurements with phase-locked PIV verified that for eight species, shown in figure 3, spinning hummingbird wings generate stable leading edge vortices. The flow fields are interpreted using vorticity plots and velocity vectors, which demonstrate that the flow is attached at 30° and 45° angle of attack, as found *in vivo* [43]. Reflections at the wing surface prohibit study of the inner

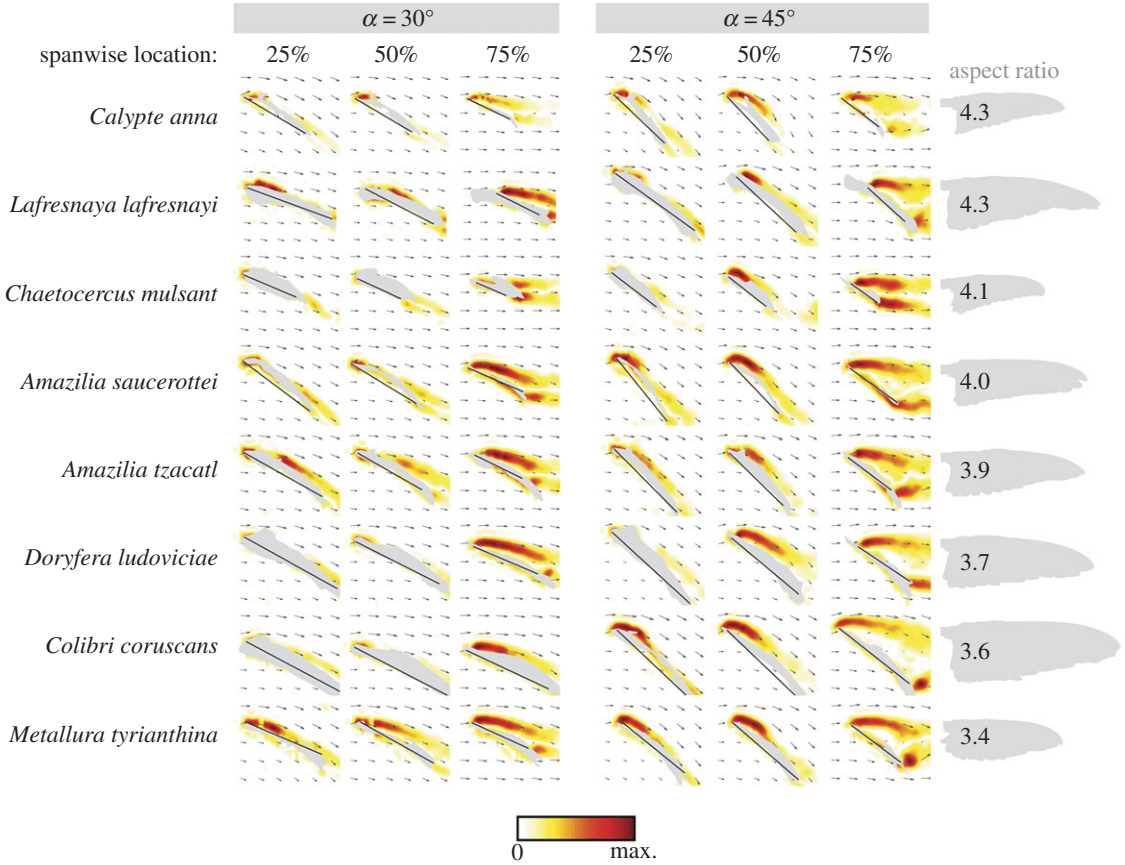

Figure 3. Flow fields around wings of eight hummingbird species at two downstroke angles of attack: $\alpha = 30^\circ$ and $\alpha = 45^\circ$ (ranked for wing aspect ratio). The vorticity and velocity fields shown represent the average for 25 phase-locked snapshots at three stations along the wing: 25%, 50% and 75% wing span (from root to tip). Absolute vorticity is shown in colour. Max (red) absolute vorticity corresponds to 17 000, 8000, 11 000, 10 000, 8000, 10 000, 10 000 and 8000 s^{-1} from top to bottom; black arrows represent local velocity vectors; grey masks cover areas in which velocity data could not be obtained due to reflection of laser light at the surface; straight black lines are plotted between the leading edge and trailing edge. (Online version in colour.)

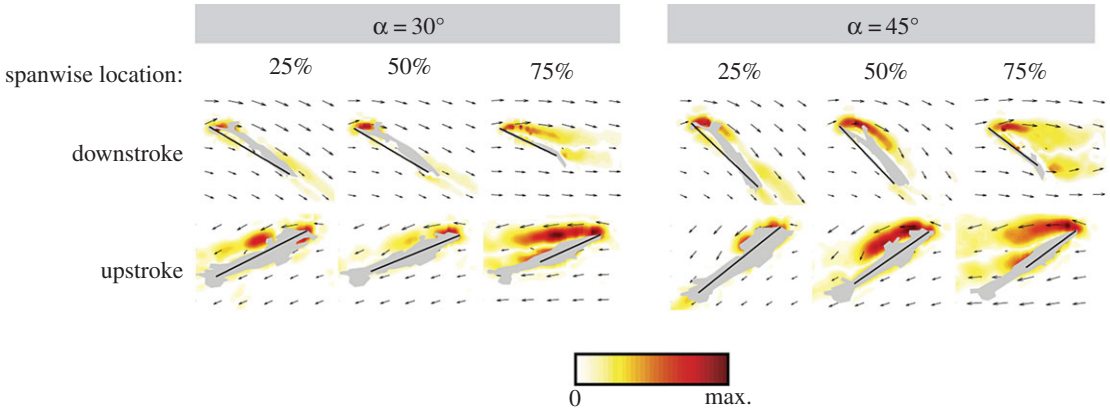

Figure 4. Flow fields around a *Calypte anna* wing during the downstroke and upstroke show that the inverted wing continues to generate a stable leading edge vortex. Angle of attack is $\alpha = \pm 30^\circ$ and $\alpha = \pm 45^\circ$. The vorticity and velocity fields shown represent the average for 25 phase-locked snapshots at three stations along the wing: 25%, 50% and 75% wing span (from root to tip). Max (red) absolute vorticity corresponds to 17 000 s^{-1}. The wing stations, velocity vectors and masks are presented as in figure 3. (Online version in colour.)

boundary layer, but at higher angles of attack the leading edge vortex is sufficiently large to be measured. Whereas the flow near the root is fully attached, the shear layer separates at 75% wingspan where it connects to the tip vortex, similar to findings for maple seeds [45]. Hummingbirds are specialized hoverers who invert their fully extended wing to generate lift during the upstroke [42,43,46]. We compared the flow fields of *C. anna* wings at both downstroke and inverted upstroke angles of attack. In both cases, we find that the airflow is attached and shows a stable leading edge vortex (figure 4). Although the flow fields suggest downstroke and upstroke symmetry, it is necessary to compare lift, drag and power measurements to determine whether aerodynamic efficacy is equivalent for the two strokes.

Similar to *in vivo* recordings [43], our quasi-steady force measurements suggest the downstroke of a hummingbird is more effective than the upstroke. For *C. anna*, we find that the maximum lift is 32% higher, whereas drag is 29% lower during the downstroke (at 45° angle of attack) compared with the inverted upstroke (at −45°). These numbers are

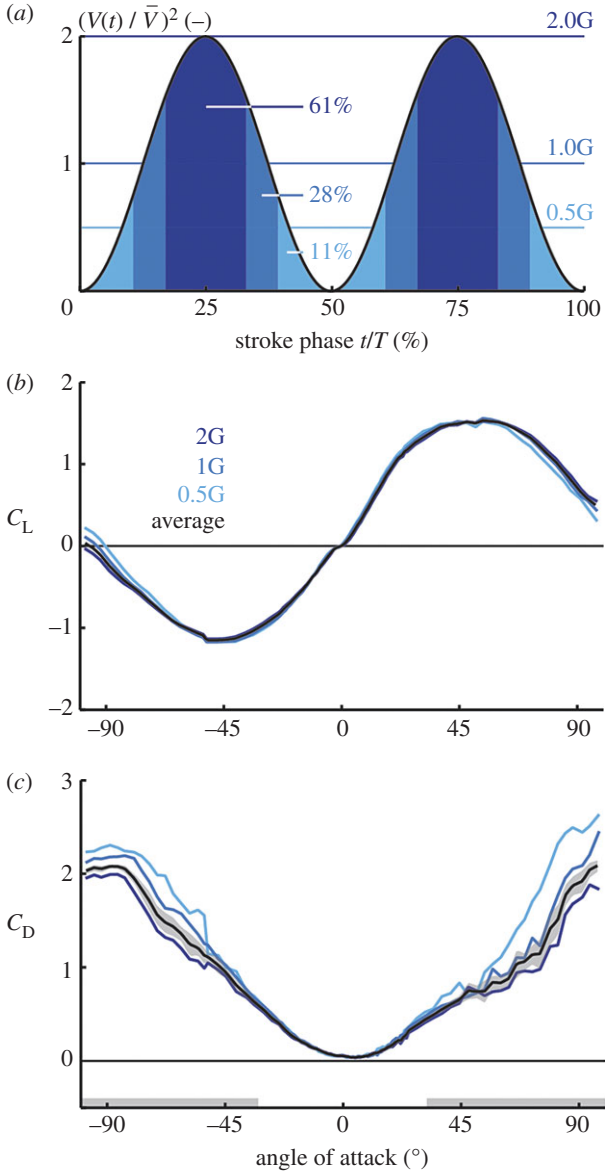

Figure 5. Lift and drag of a *Calypte anna* wing measured at three different G-loadings, which we averaged to obtain wingstroke-representative average polars (weighted by velocity squared). (*a*) Normalized instantaneous velocity squared within a *C. anna* wingbeat. Lift and drag measurements are made as a function of angle of attack for 0.5, 1 and 2G, which each represent a part of the stroke, contributing 11%, 28% and 61%, respectively, to the averaged lift and drag. (*b*,*c*) Lift and drag coefficient as a function of angle of attack for three different G-loadings. The dynamic average is shown in black and the grey band shows standard deviation. The light grey bars along the horizontal axis (in figures 5*c*, 6 and 7*g*–*i*, 8*b*–*d*, 9*c*) indicate the angle of attack range for which the set-up dynamics influenced the drag measurement (electronic supplementary material, figure S1) and thus power factor. *Calypte anna*'s angle of attack range during hovering flight is shown in figure 1*c*. (Online version in colour.)

similar to quasi-steady spinner measurements on pigeon wings [27]. Our measurements for *C. anna* wings ($-90^\circ \leq \alpha \leq 90^\circ$) show G-loading has no significant influence on lift, but drag is reduced by G-loading at angles of attack beyond roughly $\pm 45^\circ$, figure 5, likely owing to flattening of the wing under loading [36]. This result indicates that wing compliance has aerodynamic implications [36,47] for hummingbirds at angles of attack beyond 45° but not below [21]. We also note that contrary to earlier reports of negative drag coefficients at low angle of attack [24,26], we measure positive drag coefficients at all angles of attack owing to a more precise spinner design and greatly increased sampling. Our measurements represent, therefore, the most accurate drag measurements of a hummingbird wing so far. One limitation of the quasi-steady spinning wing paradigm [9,10] is that musculoskeletal actuation is ignored, which is particularly relevant during the upstroke when the wing is actively twisted [9].

Harmonic functions, which form the foundation of the quasi-steady model, fit the data for *C. anna* well (figure 6*a*). Our quasi-steady model for hummingbird flight can be used to estimate aerodynamic force and power more carefully than previous methods [19]. The harmonic fit is reasonably precise ($\varepsilon_{RMS}(C_L) = 0.031$, $\varepsilon_{RMS}(C_D) = 0.059$ for $\alpha < 0$ and $\varepsilon_{RMS}(C_L) = 0.045$, $\varepsilon_{RMS}(C_D) = 0.085$ for $\alpha \geq 0$). In contrast to insect wings [21,48], we can not assume that pressure force acts perpendicular to the projected wing surface area for hummingbirds. This is because the resultant force is rotated more than 90° forward with respect to aerodynamic angle of attack during the downstroke (figure 6*b*). The difference between results obtained with flat insect wing models and our hummingbird wings are most likely due to camber. The camber probably results in a forward-pointing suction force near the leading edge induced by the leading edge vortex, analogous to the Polhamus effect [22,49]. Comparison of the direction of the resultant force on hummingbird wings and a cambered helicopter rotor show that camber could indeed explain this difference (figure 6*c*). This rotated resultant force corresponds to a reduction in pressure drag at high angles of attack. By contrast, the resultant force vector *is* rotated over 90° with respect to aerodynamic angle of attack when the hummingbird wings and helicopter rotor are inverted. When the wing is inverted, camber cannot contribute to lift and does not project the suction force induced by the leading edge vortex forward (figure 6*c*).

We estimate the hover performance for *C. anna* by combining the quasi-steady force polar in figure 7*d* with the recorded wing kinematics in figure 1*c*. The model predicts 70% body weight support, a typical fraction for the quasi-steady model [21,22], at the cost of 0.15 W aerodynamic power. Assuming the flight muscles represent 25% of the body mass [19,50], we calculate a muscle mass (1.17 g) specific aerodynamic power of 130 W kg^{-1}. Ellington's actuator disc model [51] in combination with our morphological data for *C. anna* predicts 90 W kg^{-1}, using his generic profile drag coefficient of $C_{Dpro} = 0.075$. The same model based on $C_{Dpro} = 0.139$ measured for *Archilochus colubris* by Altshuler *et al.* [26], predicts 105 W kg^{-1}. These values are similar to Chai and Dudley's quasi-steady estimate of 100 W kg^{-1} [19] and Altshuler *et al.*'s 93 W kg^{-1} estimate for *C. anna* [2] based on Ellington's model. Our higher fidelity quasi-steady model shows the actuator disc model [51] underpredicts hover power with about 30%. The power and force asymmetry between the down versus upstroke depends primarily on angle of attack, because stroke velocity squared and wing area are similar during up and down stroke of a hummingbird [46]. For *C. anna*, we measured a mid-downstroke angle of attack of +22°, and a mid-upstroke angle of −39°, which are close to the values of +14° and −38° reported for *Selasphorus rufus* [46]. Comparing stroke halves, we find that the quasi-steady model predicts that 47% of the lift is generated during the upstroke, which is higher than the 25–33% found by Warrick *et al.* [42,43], based on *in vivo* flow analysis. According

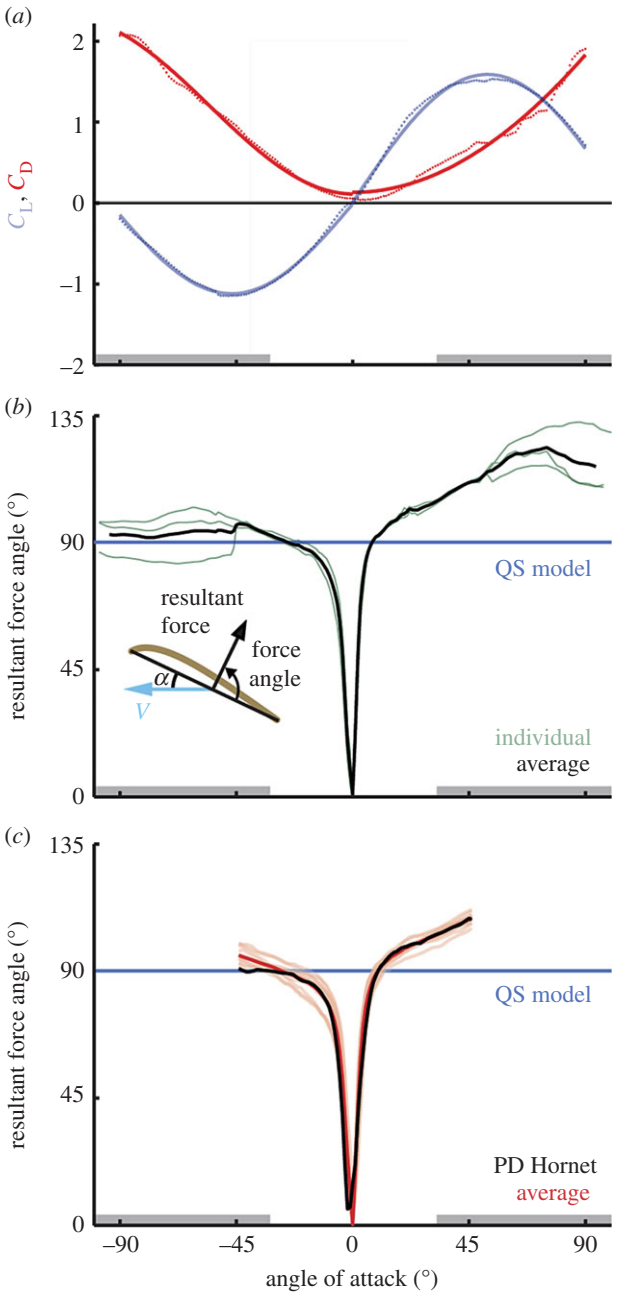

Figure 6. Quasi-steady lift and drag model approximation of hummingbird wings and a micro helicopter rotor. (*a*) First-order Fourier approximation of lift and drag coefficient versus α (G-loading averaged) shows harmonic functions approximate the data well for *Calypte anna* for $-90^\circ \leq \alpha \leq 90^\circ$ (solid line, harmonic functions; points, measurements). The harmonic functions for $\alpha < 0$ are: $C_L = 0.0028 + 1.1251\ \cos(0.0332\alpha + 4.6963)$, $C_D = 1.1993 + 1.0938\ \cos(0.0281\alpha + 3.1277)$, with accuracy $\varepsilon_{RMS}(C_L) = 0.033$, $\varepsilon_{RMS}(C_D) = 0.049$. For $\alpha \geq 0$; $C_L = 0.0031 + 1.5842\ \cos\ (0.0301\alpha + 4.7124)$, $C_D = 8.3171 + 8.1909\ \cos(0.0073\alpha + 3.1416)$, with accuracy $\varepsilon_{RMS}(C_L) = 0.048$, $\varepsilon_{RMS}(C_D) = 0.087$. (*b*) According to the quasi-steady model resulting force should be 90° rotated with respect to angle of attack, indicated with a blue line. Resultant force is 90° rotated at negative angles of attack (inverted wing) during the upstroke, but not for positive angles during the downstroke. (The cambered brown curve: sketch of the aerofoil.) (*c*) Data for 12 hummingbird species and a micro helicopter rotor (ProxDynamics Black Hornet) confirm this for $-45^\circ \leq \alpha \leq 45^\circ$. The red curve represents the hummingbird average (based on figure 9*a*), light red curves represent individual hummingbird species, and the black curve represents the micro helicopter rotor (based on figure 9*a*). (Online version in colour.)

to the quasi-steady model, the upstroke requires 275 W kg^{-1} from the supracoracoideus, while the downstroke requires 50 W kg^{-1} from the pectoralis, similar to *in vivo* measurements for pigeons [52]. The power estimate for the upstroke is probably an underestimate, because we were unable to include the higher angle of attack of the arm wing owing to twist [9]. The power estimate for the entire stroke might be too low, because spinning wings systematically underpredict the drag, and thus aerodynamic power, of flapping wings [33]. A benefit of the quasi-steady model is that it allows to predict the effect of using different angle of attack kinematics throughout the stroke while supporting the same weight (70%; the quasi-steady estimate). For this calculation, we compared different angle of attack amplitudes for the upstroke and downstroke, assuming constant weight support, constant stroke amplitude and constant flapping frequency of 39.2 Hz. The model shows that the angle of attack profile of *C. anna* coincides with an aerodynamic power minimum.

To better understand the energetic implications of the preferred angle of attacks of *C. anna* (figure 1*c*), we use the lift–drag polar (figure 7*d*,*e*) to compute power factor versus angle of attack (figure 7*g*,*h*). During mid-downstroke, *C. anna* flaps its wings close to the aerodynamically optimal angle of attack, during the rest of the stroke it flaps its wings at an aerodynamically less optimal angle of attack (figure 7*h*). We extended this analysis from a single *C. anna* specimen to five individuals, and ultimately to 12 different species of hummingbirds (figure 7). We find similar intra- and interspecies results for midstroke angles of attack between −45° and 45°. The power factor curve shows that minimum aerodynamic hover power is required at an angle of attack at 16° for *C. anna* and close to this value for all species (figure 7*i*). We found no flow separation or dominant leading edge vortex at this low angle of attack; if it is present, it is probably so close to the surface that surface reflections obscure it [43]. The absence of a prominent leading edge vortex at low angles of attack corresponds to earlier findings that at the higher Reynolds numbers of hummingbirds, a strong leading edge vortex does not correspond to minimum hover power [35]. If hummingbirds could spin their wing at a moderate angle of attack (e.g. 16°) during the whole stroke, like helicopters, they would indeed require less quasi-steady power to hover (figure 7*g*–*i*). The power factor curve also shows that although the overall flow fields of the upstroke and downstroke seem equivalent in figure 5, maximum power factor is dramatically lower during the inverted upstroke: −59% on average across hummingbirds (for 15° versus −15° angle of attack). However, hummingbirds operate their wings mostly at higher, aerodynamically suboptimal, angles of attack for which the difference between the upstroke and downstroke is somewhat smaller: −46% (for 45° versus −45° angle of attack). Considering that hummingbirds have evolved under selective pressures for hover performance, we expect that hummingbirds flap their wings at aerodynamically suboptimal angle of attack, during part of the stroke, to mitigate inertial losses and optimize muscle mechanics during forward [35] and hovering flight [19,50].

Hovering is an aerodynamically demanding flight mode, therefore we tested whether the reported variation in wing AR among hummingbirds [16,17] can predict the differences in quasi-steady aerodynamic lift, drag and efficacy (figure 7*c*,*f*,*i*). Linear regression of quasi-steady power factor with wing AR for 12 species shows that AR predicts hovering efficacy during the downstroke (figure 8). At angles of attack that correspond with the downstroke of a *C. anna* wing, we find that lift increases with AR and drag decreases somewhat

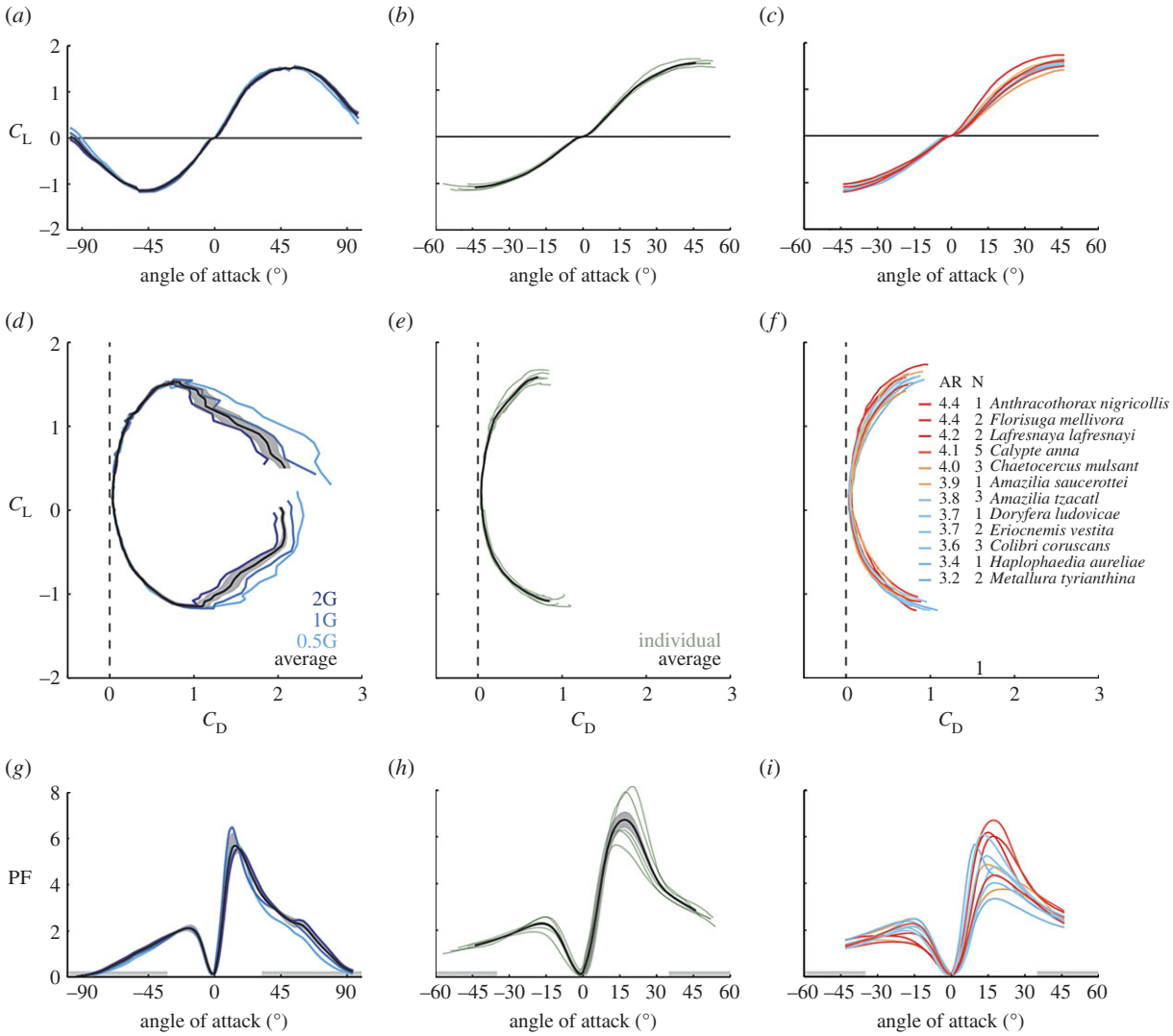

Figure 7. Lift coefficient versus angle of attack, lift–drag polars and power factor versus angle of attack for three successive levels of representation: (*a*,*d*,*g*) individual level for *Calypte anna* (G-loading averaged by weighting for velocity squared), (*b*,*e*,*h*) intraspecies level, averaged for five individuals (*C. anna*), (*c*,*f*.*i*) interspecies level, averages for different hummingbirds species colour-coded for wing aspect ratio. The dark grey band in (*a*,*b*,*d*,*e*,*g*,*h*) shows standard deviation. (Online version in colour.)

with AR, but the 95% CIs of these trends do not exclude zero (figure 8*a*,*b*). Together, however, they build up a 95% CI for power factor that does exclude zero, which shows that hummingbird wings with higher AR require less power to support body weight than wings with low AR (figure 8*c*). This trend can also be seen through visual inspection of figure 7*f* in which power factor is colour-coded based on AR. The 95% CIs of the power factors for the species whose mean power factors differ most, *C. anna* and *Haplophaedia aureliae*, are mutually exclusive for angles of attack larger than −37°. At the individual level, when not pooling the wings per species, we find the same effect of AR on power factor. Assuming the AR range of hummingbird wings facilitates efficient hovering flight, it is important to consider how current state-of-the-art micro helicopters could benefit from these biological designs, which have been optimized through more than 20 Myr of natural and sexual selection [53].

Whereas our quasi-steady aerodynamic hover power estimate gives valuable insights into the biomechanics of flapping hummingbird wings, it does not help engineers assess if these flapping wings can aerodynamically outperform spinning ones. To assess whether flapping a hummingbird wing is more efficient than spinning it like a helicopter rotor, we calculate the required power for *C. anna* wings that spin like a helicopter rotor. To estimate the aerodynamic power required to hover like a helicopter, we ignore induced flow differences between a single versus double-bladed rotor [15]. Two *C. anna* wings spinning at 44 Hz and angle of attack of 16° require only 0.048 W to lift 70% of body weight. According to our quasi-steady model, flapping a hummingbird wing requires 207% more power than spinning it to lift the same weight. To obtain a more tangible bioinspired design perspective, we tested the aerodynamic performance of the rotor of the ProxDynamics Black Hornet helicopter, which is currently employed by the British army for battlefield surveillance (http://en.wikipedia.org/wiki/Black_Hornet_Nano accessed on 27 August 2013).

Comparison of the species-average hummingbird and PD Black Hornet lift–drag polar and power factor curves shows they perform similarly (figure 9). The PD Black Hornet rotor has a somewhat more slender blade with AR 4.7 versus 3.9 for the hummingbird species average. These ARs are, however, both very small compared with large-scale helicopter rotors with ARs of about 20 [13,15]. The smaller ARs of about 4 studied here are similar to those of many toy helicopters that

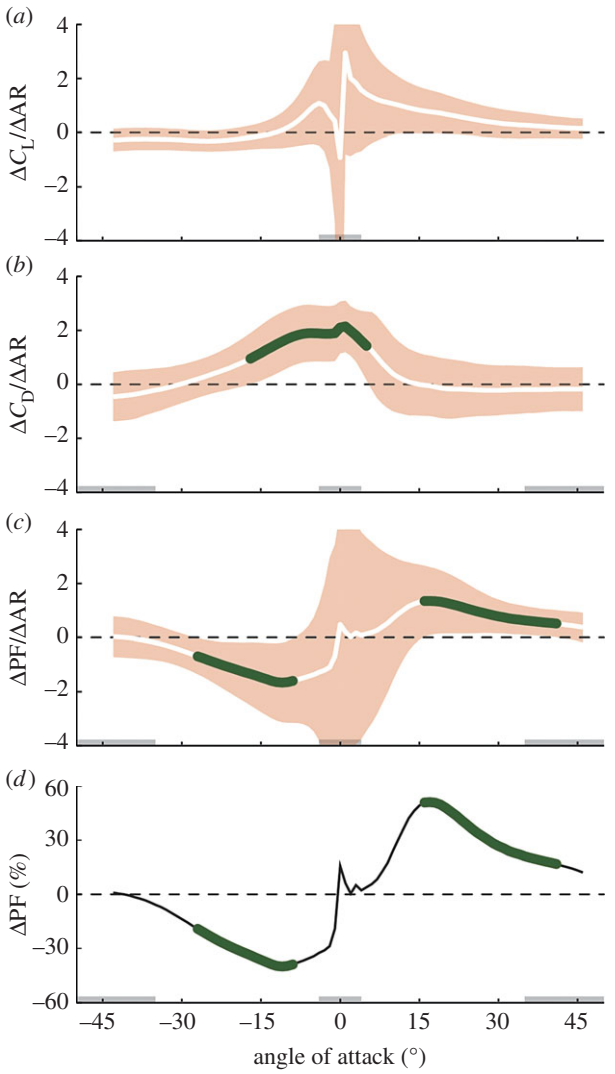

Figure 8. The influence of aspect ratio on lift, drag and power factor is dependent on the angle of attack. The *x*-axis shows the angle of attack for which we tested all wings. The *y*-axis provides the correlation coefficient between the AR and aerodynamic variable indicated. The correlations are based on the average logarithmic values for 12 hummingbird species. (*a*) The white line connects the correlation coefficients between lift and AR at each angle of attack, and the light red area represents the 95% CI. Because the CI includes 0 at all angles of attack, there is no evidence for a relationship between lift and AR. Note that the lift measurements are less precise for $-4^\circ < \alpha < 4^\circ$, indicated by the grey bar along the *x*-axis. (*b*) The green line indicates the angles of attack at which there is a significant relationship (i.e. the CI excludes 0) between drag and AR. Note that drag measurements are less precise for $-35^\circ > \alpha > 35^\circ$ (indicated with the grey bar). The influence of AR on drag is significant at low angles of attack, but hummingbirds beat their wings at higher angles (figure 1*c*). (*c*) In contrast to lift and drag, the relationship between AR and power factor is significant at high angles of attack, at which hummingbirds beat their wings during the downstroke (figure 1*c*). (*d*) The percentage of increase in (non-logarithmic) power factor from the lowest to the highest hummingbird AR, as predicted by the trend gradient in (*c*). (Online version in colour.)

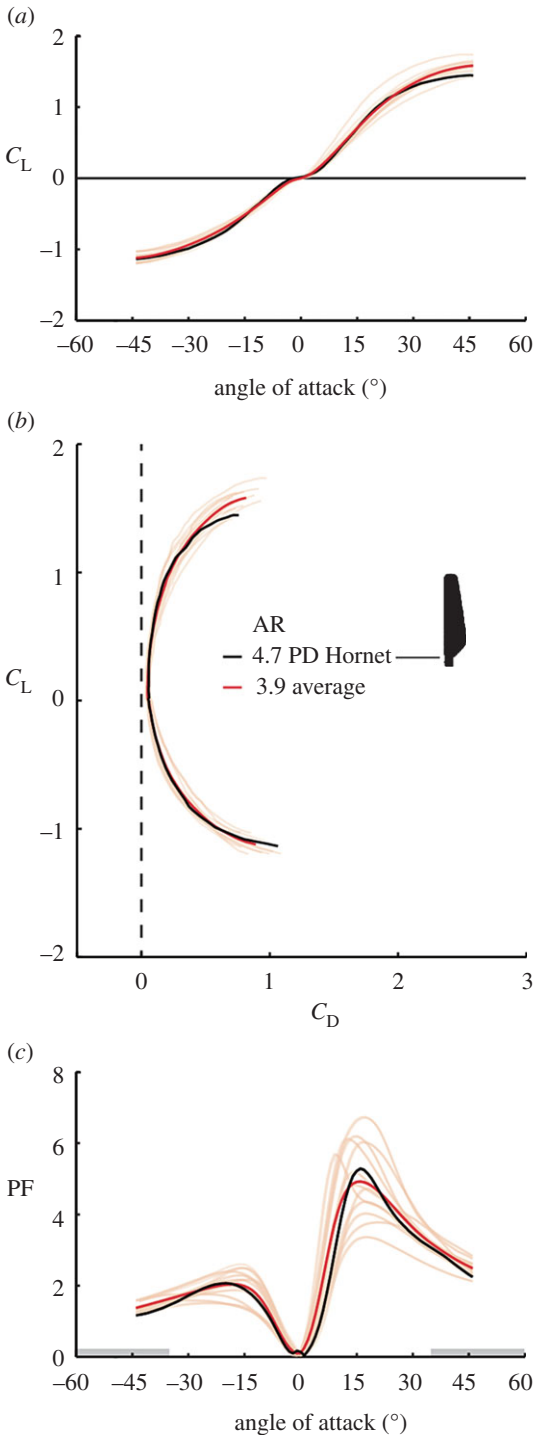

Figure 9. The average aerodynamic performance of a hummingbird wing and micro helicopter rotor (ProxDynamics Black Hornet) is equivalent. (Low intensity curves are species-averages for hummingbirds shown in figure 7*c*,*f*,*i*.) Lift coefficient (*a*) and lift–drag polar comparison (*b*) show hummingbirds generate more lift at high angles of attack. (*c*) The power factor of the average hummingbird wing is equivalent to the helicopter rotor at downstroke and upstroke angles of attack relevant for hummingbirds, and rotor angles of attack relevant for helicopters. (Online version in colour.)

are currently available on the consumer market. Apparently, micro helicopter and hummingbird wing AR converged to similar small values. The wing architecture is, however, dramatically different. The ProxDynamics Black Hornet rotor is smooth and non-porous. Hummingbird wings are composed of thin porous feathers [54] with protrusive rachises [26,55] that make the wing surface rough. Yet, the resulting lift–drag polars are surprisingly similar, except at 45° angle of attack when the average hummingbird wing generates 9% more lift (figure 9*a*). At negative angles of attack, corresponding with the inverted upstroke, the average hummingbird wing and the micro helicopter rotor perform equivalently. The best hummingbird wing, however, generates more lift and less drag at all angles of attack than the engineered rotor (figure 9*b*). To

compare hover performance, we need to compare power factor, which is equivalent for the species-averaged hummingbird wing and the helicopter rotor at all angles of attack (figure 9*c*). This finding suggests that both micro helicopter rotor design and natural selection ended up with similar aerodynamic performance for rotors and wings that need to perform well during hovering flight. It also shows that hummingbird wings can be modelled well with architecturally more simplistic engineered rotors. This insight can enable computational fluid dynamics modelling efforts and hummingbird-inspired robot design [56]. Comparison of the best performing hummingbird wing in our study with the advanced helicopter rotor (figure 9*c*) suggests that there might be an opportunity to further improve the maximum power factor of micro helicopter rotors up to 27% (compared with *C. anna*, $n = 5$). Although our quasi-steady analysis of hummingbird wings is most precise for analysing hovering flight performance, it can be used for estimating thrust vectoring during slow hovering flight, which provides a window towards assessing hummingbird manoeuvrability.

Acknowledgements. We gratefully acknowledge Eric Karruppannan, Ad Holten, Evert Janssen and Mees Muller for help with building the experimental set-up, Henk Schipper, Kees Voesenek for computing support, Gary Stiles and the Instituto de Ciencias Naturales of the Universidad Nacional de Colombia for providing the hummingbird wings of Colombian species, and Petter Muren and ProxDynamics for giving us a rotor blade of their prototype Black Hornet helicopter.

Funding statement. The research was supported by NWO-ALW grant no. 817.02.012 to J.W.K. and D.L. and a JEB travel fellowship and a WIAS junior fellowship to E.M.Q.R. D.L.A. was supported by a WIAS travel grant from Wageningen University and a United States National Science Foundation grant (no. IOS 0923849).

References

1. Clark CJ. 2011 Wing, tail, and vocal contributions to the complex acoustic signals of courting Calliope hummingbirds. *Curr. Zool.* **57,** 2507–2514.
2. Altshuler DL, Welch KC, Cho BH, Welch DB, Lin AF, Dickson WB, Dickinson MH. 2010 Neuromuscular control of wingbeat kinematics in Anna's hummingbirds (*Calypte anna*). *J. Exp. Biol.* **213**, 2507–2514. (doi:10.1242/jeb.043497)
3. Rome LC. 2006 Design and function of superfast muscles: new insights into the physiology of skeletal muscle. *Annu. Rev. Physiol.* **68**, 193–221. (doi:10.1146/annurev.physiol.68.040104.105418)
4. Greenewalt CH. 1975 The flight of birds: the significant dimensions, their departure from the requirements for dimensional similarity, and the effect on flight aerodynamics of that departure. *Trans. Am. Philos. Soc.* **65**, 1–67. (doi:10.2307/1006161)
5. Suarez R. 1992 Hummingbird flight: sustaining the highest mass-specific metabolic rates among vertebrates. *Experientia* **48**, 565–570. (doi:10.1007/BF01920240)
6. Wells DJ. 1993 Muscle performance in hovering hummingbirds. *J. Exp. Biol.* **178**, 39–57.
7. Zusi RL. 2013 Introduction to the skeleton of hummingbirds (aves: Apodiformes, Trochilidae) in functional and phylogenetic contexts. *Ornithol. Monogr.* **77**, 1–94. (doi:10.1525/om.2013.77.1.1)
8. Mathieu-Costello O, Suarez R, Hochachka P. 1992 Capillary-to-fiber geometry and mitochondrial density in hummingbird flight muscle. *Respir. Physiol.* **89**, 113–132. (doi:10.1016/0034-5687(92)90075-8)
9. Hedrick TL, Tobalske BW, Ros IG, Warrick DR, Biewener AA. 2012 Morphological and kinematic basis of the hummingbird flight stroke: scaling of flight muscle transmission ratio. *Proc. R. Soc. B* **279**, 1986–1992. (doi:10.1098/rspb.2011.2238)
10. Welch Jr KC, Altshuler DL. 2009 Fiber type homogeneity of the flight musculature in small birds. *Comp. Biochem. Physiol. B, Biochem. Mol. Biol.* **152**, 324–331. (doi:10.1016/j.cbpb.2008.12.013)
11. Donovan ER, Keeney BK, Kung E, Makan S, Wild JM, Altshuler DL. 2013 Muscle activation patterns and motor anatomy of Anna's hummingbirds *Calypte anna* and zebra finches *Taeniopygia guttata*. *Physiol. Biochem. Zool.* **86**, 27–46. (doi:10.1086/668697)
12. Prandtl L, Tietjens OKG. 1957 *Applied hydro- and aeromechanics: based on lectures of L. Prandtl, PhD*, vol. 2. Mineola, New York: Dover Publications.
13. Stepniewski WZ. 1984 *Rotary-wing aerodynamics*. Mineola, NY: Courier Dover Publications.
14. Anderson JD. 2001 *Fundamentals of aerodynamics*, vol. 2. New York, NY: McGraw-Hill.
15. Leishman JG. 2006 *Principles of helicopter aerodynamics*. Cambridge, UK: Cambridge University Press.
16. Altshuler DL. 2001 Ecophysiology of hummingbird flight along elevational gradients: an integrated approach. PhD thesis, University of Texas at Austin, Austin.
17. Stiles FG. 1995 Behavioral, ecological and morphological correlates of foraging for arthropods by the hummingbirds of a tropical wet forest. *Condor* 853–878. (doi:10.2307/1369527)
18. Thomas F, Milgram J. 1999 *Fundamentals of sailplane design*. College Park, MD: College Park Press.
19. Chai P, Dudley R. 1995 Limits to vertebrate locomotor energetics suggested by hummingbirds hovering in heliox. *Nature* **377**, 722–725. (doi:10.1038/377722a0)
20. Pournazeri S, Segre PS, Princevac M, Altshuler DL. 2013 Hummingbirds generate bilateral vortex loops during hovering: evidence from flow visualization. *Exp. Fluids* **54**, 1–11. (doi:10.1007/s00348-012-1439-5)
21. Dickinson MH, Lehmann F-O, Sane SP. 1999 Wing rotation and the aerodynamic basis of insect flight. *Science* **284**, 1954–1960. (doi:10.1126/science.284.5422.1954)
22. Sane SP. 2003 The aerodynamics of insect flight. *J. Exp. Biol.* **206**, 4191–4208. (doi:10.1242/jeb.00663)
23. Usherwood JR, Ellington CP. 2002 The aerodynamics of revolving wings I. Model hawkmoth wings. *J. Exp. Biol.* **205**, 1547–1564.
24. Usherwood JR, Ellington CP. 2002 The aerodynamics of revolving wings II. Propeller force coefficients from mayfly to quail. *J. Exp. Biol.* **205**, 1565–1576.
25. Usherwood JR. 2009 The aerodynamic forces and pressure distribution of a revolving pigeon wing. *Exp. Fluids* **46**, 991–1003. (doi:10.1007/s00348-008-0596-z)
26. Altshuler DL, Dudley R, Ellington CP. 2004 Aerodynamic forces of revolving hummingbird wings and wing models. *J. Zool.* **264**, 327–332. (doi:10.1017/S0952836904005813)
27. Crandell KE, Tobalske BW. 2011 Aerodynamics of tip-reversal upstroke in a revolving pigeon wing. *J. Exp. Biol.* **214**, 1867–1873. (doi:10.1242/jeb.051342)
28. McGuire JA *et al*. 2014 Molecular phylogenetics and the diversification of hummingbirds. *Curr. Biol.* **24**, 910–916. (doi:10.1016/j.cub.2014.03.016)
29. Dial TR, Heers AM, Tobalske BW. 2012 Ontogeny of aerodynamics in mallards: comparative performance and developmental implications. *J. Exp. Biol.* **215**, 3693–3702. (doi:10.1242/jeb.062018)
30. Altshuler D, Dudley R, Heredia S, McGuire J. 2010 Allometry of hummingbird lifting performance. *J. Exp. Biol.* **213**, 725–734. (doi:10.1242/jeb.037002)
31. Altshuler DL, Quicazán-Rubio EM, Segre PS, Middleton KM. 2012 Wingbeat kinematics and motor control of yaw turns in Anna's hummingbirds (*Calypte anna*). *J. Exp. Biol.* **215**, 4070–4084. (doi:10.1242/jeb.075044)
32. Weis-Fogh T. 1973 Quick estimates of flight fitness in hovering animals, including novel mechanisms for lift production. *J. Exp. Biol.* **59**, 169–230.
33. Sane SP, Dickinson MH. 2001 The control of flight force by a flapping wing: lift and drag production. *J. Exp. Biol.* **204**, 2607–2626.
34. Dickson WB, Straw AD, Dickinson MH. 2008 Integrative model of *Drosophila* flight. *AIAA J.* **46**, 2150–2164. (doi:10.2514/1.29862)

35. Lentink D, Dickinson MH. 2009 Rotational accelerations stabilize leading edge vortices on revolving fly wings. *J. Exp. Biol.* **212**, 2705–2719. (doi:10.1242/jeb.022269)
36. Zhao L, Huang Q, Deng X, Sane SP. 2010 Aerodynamic effects of flexibility in flapping wings. *J. R. Soc. Interface* **7**, 485–497. (doi:10.1098/rsif.2009.0200)
37. Lentink D *et al*. 2007 How swifts control their glide performance with morphing wings. *Nature* **446**, 1082–1085. (doi:10.1038/nature05733)
38. Wang ZJ. 2008 Aerodynamic efficiency of flapping flight: analysis of a two-stroke model. *J. Exp. Biol.* **211**, 234–238. (doi:10.1242/jeb.013797)
39. Eilers PH. 2003 A perfect smoother. *Anal. Chem.* **75**, 3631–3636. (doi:10.1021/ac034173t)
40. Poelma C, Dickson W, Dickinson M. 2006 Time-resolved reconstruction of the full velocity field around a dynamically-scaled flapping wing. *Exp. Fluids* **41**, 213–225. (doi:10.1007/s00348-006-0172-3)
41. Fry SN, Sayaman R, Dickinson MH. 2003 The aerodynamics of free-flight maneuvers in *Drosophila*. *Science* **300**, 495–498. (doi:10.1126/science.1081944)
42. Warrick DR, Tobalske BW, Powers DR. 2005 Aerodynamics of the hovering hummingbird. *Nature* **435**, 1094–1097. (doi:10.1038/nature03647)
43. Warrick DR, Tobalske BW, Powers DR. 2009 Lift production in the hovering hummingbird. *Proc. R. Soc. B* **276**, 3747–3752. (doi:10.1098/rspb.2009.1003)
44. Ellington CP, van den Berg C, Willmott AP, Thomas ALR. 1996 Leading-edge vortices in insect flight. *Nature* **384**, 626–630. (doi:10.1038/384626a0)
45. Lentink D, Dickson WB, van Leeuwen JL, Dickinson MH. 2009 Leading-edge vortices elevate lift of autorotating plant seeds. *Science* **324**, 1438–1440. (doi:10.1126/science.1174196)
46. Tobalske BW, Warrick DR, Clark CJ, Powers DR, Hedrick TL, Hyder GA, Biewener AA. 2007 Three-dimensional kinematics of hummingbird flight. *J. Exp. Biol.* **210**, 2368–2382. (doi:10.1242/jeb.005686)
47. Young J, Walker SM, Bomphrey RJ, Taylor GK, Thomas AL. 2009 Details of insect wing design and deformation enhance aerodynamic function and flight efficiency. *Science* **325**, 1549–1552. (doi:10.1126/science.1175928)
48. Birch JM, Dickson WB, Dickinson MH. 2004 Force production and flow structure of the leading edge vortex on flapping wings at high and low Reynolds numbers. *J. Exp. Biol.* **207**, 1063–1072. (doi:10.1242/jeb.00848)
49. Polhamus EC. 1971 Predictions of vortex-lift characteristics by a leading-edge suctionanalogy. *J. Aircraft* **8**, 193–199. (doi:10.2514/3.44254)
50. Chai P, Dudley R. 1996 Limits to flight energetics of hummingbirds hovering in hypodense and hypoxic gas mixtures. *J. Exp. Biol.* **199**, 2285–2295.
51. Ellington C. 1984 The aerodynamics of hovering insect flight. VI. Lift and power requirements. *Phil. Trans. R. Soc. Lond B* **305**, 145–181. (doi:10.1098/rstb.1984.0054)
52. Tobalske BW, Biewener AA. 2008 Contractile properties of the pigeon supracoracoideus during different modes of flight. *J. Exp. Biol.* **211**, 170–179. (doi:10.1242/jeb.007476)
53. Bleiweiss R. 1998 Tempo and mode of hummingbird evolution. *Biol. J. Linn. Soc.* **65**, 63–76. (doi:10.1111/j.1095-8312.1998.tb00351.x)
54. Muller W, Patone G. 1998 Air transmissivity of feathers. *J. Exp. Biol.* **201**, 2591–2599.
55. Elimelech Y, Ellington CP. 2013 Analysis of the transitional flow field over a fixed hummingbird wing. *J. Exp. Biol.* **216**, 303–318. (doi:10.1242/jeb.075341)
56. Keennon M, Klingebiel K, Won H, Andriukov A. 2012 In *50th AIAA Aerospace Sciences Meeting including the New Horizons Forum and Aerospace Exposition*, pp. 1–24.